Negative permittivity of ZnO thin films prepared from aluminum and gallium doped ceramics via pulsed-laser deposition

M.A. Bodea[1, +], G. Sbarcea[1,2,3, +], G.V. Naik[4], A. Boltasseva[4,5,6], T.A. Klar[1], J.D. Pedarnig[1,*]

[1] Institute of Applied Physics, Johannes Kepler University Linz, 4040 Linz, Austria

[2] University Politehnica of Bucharest, 060042 Bucharest, Romania

[3] National Institute for Research and Development in Electrical Engineering ICPE-CA, 030138 Bucharest, Romania

[4] School of Electrical and Computer Engineering and Birck Nanotechnology Center, Purdue University, West Lafayette, Indiana 47907, USA

[5] DTU Fotonik, Technical University of Denmark, Kgs. Lyngby DK 2800, Denmark

[6] Erlangen Graduate School of Advanced Optical Technologies (SAOT), University Erlangen Nürnberg, 91052 Erlangen, Germany

NOTE:

This manuscript is published by Springer in Applied Physics A:

Negative permittivity of ZnO thin films prepared from aluminum and gallium doped ceramics via pulsed-laser deposition

M.A. Bodea, G. Sbarcea, G.V. Naik, A. Boltasseva, T.A. Klar, J.D. Pedarnig

Applied Physics A 110, 929–934 (2013)

http://dx.doi.org/10.1007/s00339-012-7198-6

(Published online: 13 September 2012)

ABSTRACT

Aluminum and gallium doped zinc oxide thin films with negative dielectric permittivity in the near infrared spectral range are grown by pulsed laser deposition. Composite ceramics comprising ZnO and secondary phase Al_2O_3 or Ga_2O_3 are employed as targets for laser ablation. Films deposited on glass from dense and small-grained ceramic targets show optical transmission larger than 70 % in the visible and reveal an onset of metallic reflectivity in the near infrared at 1100 nm and a crossover to a negative real part of the permittivity at approximately 1500 nm. In comparison to noble metals, doped ZnO shows substantially smaller losses in the near infrared.

KEY WORDS: Pulsed-laser deposition, thin films, metal doped zinc oxide, spectroscopic ellipsometry, plasma frequency, plasmonics

* Corresponding author: johannes.pedarnig@jku.at, http://www.jku.at/applphys

+ Both authors (M.A.B. and G.S.) contributed equally to this study.

1. Introduction

Zinc oxide (ZnO) is a versatile material that develops different functionalities upon doping. Piezoelectricity, ferroelectricity, ferromagnetism, and electrical conductivity can be induced in ZnO depending on the type and concentration of the dopant element (e.g., Al, Co, Ga, Li, Mn) [1, 2]. Thin films of ZnO are of interest for various applications such as piezoelectric sensing devices, semiconductor p-n junctions, ultraviolet (UV) solid state lasers, and low-loss optical waveguides and amplifiers [3]. Metal doping yields thin films of high electrical conductivity and high optical transparency in the visible (VIS) spectral range suitable for transparent conductive oxide coatings [4]. Aluminum doped ZnO (Al:ZnO) thin films are reported to have charge carrier concentrations n and Hall mobilities μ at room temperature of up to 1×10^{21} cm^{-3} and 65 cm^2/Vs, respectively [5, 6, 7, 8, 9, 10, 11, 12]. Gallium doping is reported to yield Ga:ZnO films with $n \leq 1.5\times10^{22}$ cm^{-3} and $\mu \leq 30$ cm^2/Vs [6, 12, 13, 14, 15]. The plasma frequency at this carrier density is in the near infrared (NIR) spectral range. This indicates that M:ZnO (M being either Al or Ga) has metal-like optical properties like a negative dielectric permittivity $Re(\varepsilon) = \varepsilon' < 0$ and a high reflectivity in the NIR (below the plasma frequency). M:ZnO, therefore, is a candidate material to replace noble metals for plasmonic applications in the NIR [16, 17, 18]. Silver and gold are widely used for plasmonics in the VIS range but show significant losses at longer wavelengths λ. For bulk silver, the imaginary part of the dielectric permittivity $Im(\varepsilon)$ is $\varepsilon'' = 0.5$ at $\lambda = 0.6$ μm and it increases to $\varepsilon'' = 3$ at $\lambda = 1.5$ μm. As the absorption loss n'' increases with ε'' silver cannot be used at longer wavelengths for many applications (n'' is the imaginary part of the complex refractive index $n' + i \times n''$). NIR plasmonics based on low-loss materials is of interest for many applications, e.g. in nano-photonics, metamaterials, optoelectronics, telecommunications, and molecular sensing. M:ZnO thin films can be grown by various techniques including pulsed-laser deposition (PLD) and sputtering [4]. For the optimization of growth conditions, PLD is advantageous because of its versatility and the relatively high deposition rates that can be achieved. For the fabrication of large area coatings and layer growth on non-planar substrates sputtering techniques are advantageous.

In this study, we report on the growth and optical characterization of Al:ZnO and Ga:ZnO thin films with metallic properties in the NIR. PLD is employed to fabricate film samples from sintered ceramics comprising ZnO and Al_2O_3 or Ga_2O_3. Sample properties are investigated in detail by optical transmission spectrophotometry and spectroscopic

ellipsometry (SE) measurements. We show that M:ZnO thin films have negative real permittivity and small imaginary permittivity in the NIR range.

2. Experimental

The M:ZnO ceramics are prepared by mixing of pure ZnO and M_2O_3 powders, manual grinding of powder mixtures (30 min), pressing of powders to pellets (pressure of 3.5 tons/cm^2), and sintering of pellets in air. The powders used are pure ZnO (Alfa Aesar, purity 99.99 %, particle size ≤ 1 µm), Al_2O_3 (Alfa Aesar, 99.5 %, ~ 10 - 30 µm; or Acros Organics, 99.99 %, ≤ 1 µm), and Ga_2O_3 (Alfa Aesar, 99.99 %, ≤ 1 µm). The particle size of the powders was measured by optical microscopy (with 1000× magnification). The amount of M_2O_3 powder is varied (0 - 5 wt% Al_2O_3; 0 - 7 wt% Ga_2O_3) to produce ceramics of different M_2O_3 concentration. The sintering temperature and time are in the range from 600 to 1000 °C and from 2 to 16 hours, respectively. Table 1 summarizes fabrication parameters and selected properties for some of the 40 ceramics produced. The color and mass density of ceramics depends on the sintering parameters and the type of M_2O_3 powders used. Sintering at 900 - 1000 °C for 2 to 5 hours produces yellowish ceramics of Ga_2O_3/ZnO. The Al_2O_3/ZnO ceramics prepared under the same conditions are yellowish only when the finer Al_2O_3 powder is used. Dense green and grey-colored ceramics are fabricated using the coarser Al_2O_3 powder. Lower sintering temperature produces white ceramics of low density. The different color may be due to size effects and crystal defects in the oxide constituents.

For film growth, the ceramics are laser ablated by focusing the pulsed radiation of a KrF excimer laser (λ = 248 nm, pulse duration 20 ns, fluence 2 J/cm^2, pulse repetition rate 10 Hz) onto the oxide targets [19]. Films are deposited on glass and fused quartz (herasil) substrates at substrate temperature T_S = 20 – 500 °C. An oxygen gas background with pressure $p(O_2) = 10^{-3}$ mbar is employed during PLD and post-deposition cool-down. The layer thickness typically is around 350 nm for 15000 pulses.

3. Results and discussion

The PLD films show smooth surface morphology and low coverage by particulates and droplets. The surface roughness measured by atomic force microscopy depends on the substrate temperature and is R_a ~ 5 nm for samples deposited at T_S = 20 °C and R_a ~ 1

nm for T_S > 300 °C. X-ray diffraction measurements reveal a polycrystalline structure of films and an average crystallite diameter of less than 20 nm for all the samples. Films deposited at $T_S \geq 300$ °C develop strong c-axis texture perpendicular to the substrate with a pronounced (002) diffraction peak and small angular spread $\Delta\chi(002) < 20$ °. Films deposited at room temperature do not show preferential lattice orientation. The XRD data do not show peaks for metallic Al and Ga. The electrical resistivity of M:ZnO layers produced from ceramics with 2 - 3 wt% Al_2O_3 and 2 - 4 wt% Ga_2O_3 at $T_S = 300$ °C is ρ(300 K) ~ 0.5 mΩ cm. M:ZnO samples grown at T_S = 20 °C show two times higher resistivity. Undoped ZnO thin films have ρ(300 K) ~ 12 and 15 mΩ cm at substrate temperature of 20 and 300 °C, respectively.

The optical transmission of Al:ZnO and Ga:ZnO films on glass substrates is shown in Figure 1. The layers are deposited at T_s = 300 °C employing yellowish ceramics with 3 wt% M_2O_3 for ablation. In the visible, the transmission is high (T > 0.7) and shows oscillatory behavior due to Fabry-Perot interference. In the NIR range, the transmission starts to drop rapidly at λ ~ 1 µm and becomes vanishingly small at λ ~ 3 µm for both samples. Pure (un-doped) ZnO films reveal oscillatory transmission over the entire range without drop in the NIR. Similar behavior in the VIS and NIR ranges is observed for all films produced from ceramics containing 2 - 5 wt% Al_2O_3 and 2 - 7 wt% Ga_2O_3. The drop in NIR transmission is shifted to longer wavelength (λ ~ 1.2 µm) for targets with only 1 wt% concentration. In the UV, films absorb strongly due to direct interband transitions. The absorption edge in the UV is blue-shifting monotonously with increasing concentration of M_2O_3. The optical bandgap energy E_g, as derived from Tauc plots [20], is 3.28 eV (0 wt%), 3.75 (2 wt%), 3.85 (3 wt%), and 3.88 eV (5 wt%) for both metal dopants. The larger E_g for higher dopant concentration is probably related to an increasing occupancy of electronic and hole states in the conduction and valence bands, respectively (Burstein-Moss effect) [5, 12]. The transmission spectra of M:ZnO films on fused quartz substrates are very similar to the spectra of films on glass. A strong decrease of the optical transmission of Al:ZnO films in the NIR has been reported for samples with concentration of 0.8 wt % [8] and 1.8 wt % [7]. Interference fringes in the VIS range are observed also for multilayer structures consisting of differently doped ZnO films [20].

We compare the measured optical transmission spectra with spectra that are calculated assuming homogeneous films, perpendicular incidence of light, and air as ambient medium. Interference of optical waves in the layer and multiple reflections in the glass

substrate are taken into account. The dielectric permittivities of un-doped pure ZnO and of glass are taken from references [21, 22] and both materials are considered to be non-absorbing ($\varepsilon'' = 0$). Metal doping produces a free electron gas (EG) with plasma frequency ω_p and damping constant γ in the host oxide material. The dielectric susceptibility of the doped M:ZnO material is a linear superposition of the susceptibilities of host material and the EG. The calculated optical transmission for the Al:ZnO thin film shows oscillations in the VIS and a drop of transmission in the NIR similar to the measured data (solid line "sim1", Fig. 1a). The parameters employed in the calculation are a layer thickness d of 300 nm and plasma parameters $\omega_p = 2.1\times10^{15}$ s^{-1} and $\gamma = 3.5\times10^{14}$ s^{-1}. With these parameters, the calculated dielectric permittivity of the film at $\lambda = 1.5$ µm is $\varepsilon_{Al:ZnO} = 0.94 + i\times0.72$. The permittivity of un-doped pure ZnO is 3.53 at this wavelength [21]. The corresponding concentration of free charge carriers $n = \left(\omega_p / e\right)^2 \varepsilon_0 \, m^*$ and the carrier mobility at zero frequency $\mu_{DC} = e/\left(m^* \gamma\right)$ in Al:ZnO are n = 3.7×10^{20} cm^{-3} and μ_{DC} = 19.0 cm^2/Vs, respectively. The effective optical mass of electrons is $m^* = 0.265\ m_0$ [23] with m_0 the free electron mass, e is the elementary charge unit and ε_0 the permittivity of vacuum. For the Ga:ZnO film, the transmission is calculated for d = 370 nm, $\omega_p = 2.4\times10^{15}$ s^{-1} and $\gamma = 2.75\times10^{14}$ s^{-1} (solid line "sim1", Fig. 1b). The permittivity at $\lambda = 1.5$ µm is $\varepsilon_{Ga:ZnO} = 0.047 + i\times0.76$. The charge density and mobility are n = 4.8×10^{20} cm^{-3} and μ_{DC} = 24.1 cm^2/Vs, respectively. For pure ZnO films, i.e. with $\omega_p = \gamma = 0$, the calculated transmissions remain at high value (dashed lines "sim2" in Fig. 1a and Fig. 1b). The good agreement of measured and simulated optical transmission spectra shows that the blocking of NIR transmission results from the EG in the metal doped oxide film. Advanced modeling of transmission spectra including interband transitions in the UV and intraband excitations of the EG with frequency dependent damping $\gamma(\omega)$ results in a better match of measured and calculated spectra [24]. In this case, a charge density (8.8×10^{20} cm^{-3}) and mobility (μ = 36 cm^2/Vs) for sputter-deposited Al:ZnO films (2 wt%) larger than our results have been obtained.

For more detailed investigations of the optical properties, the thin film samples are analyzed by spectroscopic ellipsometry (SE, [25]). Figure 2 shows the SE parameters Δ and Ψ of an Al:ZnO film (ceramic with 2 wt% Al_2O_3) on glass measured for two different angles of incidence (AOI = 60° and 70°). The parameter Δ shows phase changes by 2π at wavelengths of 521 and 758 nm (for AOI = 60°). Dashed lines show fits to the data using a model for the dielectric function of the Al:ZnO film. The model comprises one Lorentz

oscillator, one Drude term, and a constant background permittivity ε_∞. The resonance energy of the Lorentz oscillator is set to 3.7 eV in correspondence to the interband absorption. The amplitude and damping constants of Lorentz oscillator and Drude term and the permittivity ε_∞ are fit parameters. The layer thickness is set to 380 nm as derived from the interference fringes in the VIS range of the transmission spectra by the PARAV program [26]. The fit matches the measured data reasonably well. The mean square error is MSE < 50 for a fit over the whole wavelength range. Better fitting and smaller error (MSE ~ 25) are achieved by using additional Lorentz oscillators and by taking into account layer roughness and thickness non-uniformity. Qualitatively similar SE data are measured also for the Ga:ZnO film on glass (ceramic with 2 wt% Ga_2O_3, data not shown). The obtained values for the amplitude and damping constants of Lorentz and Drude contributions are different for the Al:ZnO and Ga:ZnO films. M:ZnO films on fused quartz substrates have lower quality than films on glass because of a strong and peaked depolarization signal (15 - 100 %) in the range 1.25 - 1.55 µm with a width $\Delta\lambda_{FWHM} \approx 100$ nm depending on dopant concentration (1 - 7 wt%).

From the fits to measured SE data, the complex dielectric permittivity of Al:ZnO and Ga:ZnO thin films (2 wt%) on glass substrates is calculated. For both film materials, the real part $\varepsilon'_{M:ZnO}$ decreases with longer wavelengths and a transition to negative permittivity is observed at crossover wavelengths λ_c(Al:ZnO) = 1.61 µm and λ_c(Ga:ZnO) = 1.55 µm (Figure 3). The imaginary part of the dielectric permittivity increases with increasing wavelength in the NIR. At λ_c it is $\varepsilon''_{Al:ZnO}$ = 0.46 and $\varepsilon''_{Ga:ZnO}$ = 0.53 for the Al and Ga doped layers, respectively. The permittivity of undoped ZnO films deposited from pure targets (0 wt% of Al or Ga) is $\varepsilon'_{ZnO} > 3.5$ and $\varepsilon''_{ZnO} < 0.1$ in the NIR. SE analyses of epitaxial Al:ZnO films (2-3 wt%) on sapphire crystal substrates show similar dispersion of the dielectric permittivity [27, 28]. Figure 4 compares the λ_c and the imaginary permittivity $\varepsilon''(\lambda_c)$ of Al:ZnO and Ga:ZnO thin films on glass. Samples of different M_2O_3 concentration are analyzed by SE and the data are taken from the fitted permittivities. Ga doping results in shorter crossover wavelengths for all concentrations compared to Al doping. At low concentrations (2 - 4 wt%) the values of $\varepsilon''(\lambda_c)$ are comparable for both materials. The Al:ZnO and Ga:ZnO films produced from targets with 3 wt% M_2O_3 have the shortest λ_c of 1.55 µm and 1.43 µm, respectively. The permittivity ε'' is 0.55 for both materials. The mechanisms leading to the observed concentration dependence of λ_c and $\varepsilon''(\lambda_c)$ remain to be clarified. The crossover wavelengths are shorter than the “plasma wavelengths” of

Al:ZnO films reported by Kim et al [8]. The values for λ_c and $\varepsilon''(\lambda_c)$ derived from calculated optical transmission spectra (Figure 1) are 1.78 µm and 1.17 for Al:ZnO, and 1.52 µm and 0.79 for Ga:ZnO, respectively. The crossover wavelength can be estimated from the transmission spectra. The quantitative determination of λ_c and $\varepsilon''(\lambda_c)$ requires SE analysis of film samples.

The optical properties of M:ZnO films strongly depend on the type of ceramic employed as ablation target. Ceramics of the same nominal M_2O_3 concentration prepared under different conditions yield films with different properties (Table 1). Films with metal-like properties and low losses (i.e., low optical transmission and small imaginary permittivity) in the NIR and with short crossover wavelengths are achieved only with yellowish ceramics. For comparison, Al:ZnO films (4 wt%) deposited on glass from yellowish and green-colored ceramics have transmission T(λ = 1.5 µm) = 0.32 and 0.56 and crossover wavelengths λ_c = 1.61 µm and >1.7 µm, respectively. The grain size and connectivity and the defect structure of oxide constituents in ceramics is influenced by the fabrication procedure. Together with the different optical absorption of ZnO and M_2O_3 at the laser wavelength, this may lead to significant variation in amount, type, and kinetic energy of ablated species and thus modify the material properties of the condensed layer.

ZnO forms many different nanostructures such as belts, rings, combs, helices, springs, wires, cages, and vertical quantum well structures [29, 30, 31]. Metal doped M:ZnO nanostructures may reveal photonic properties that deviate from the properties of planar extended layers. M:ZnO nanomaterials may be investigated in another study. Besides oxide semiconductors, also other materials like transition metal nitrides and III-V semiconductors are of interest for NIR plasmonic applications [16].

4. Conclusions

Al and Ga doped ZnO thin films are good candidates for improved NIR plasmonic materials. More than 80 M:ZnO film samples are grown by PLD on amorphous glass and quartz substrates. High optical quality layers are produced by ablating fine-grained and dense ZnO ceramics containing Al_2O_3 or Ga_2O_3 as secondary phase. The M:ZnO films reveal negative real permittivity $\varepsilon' < 0$ and small imaginary permittivity $\varepsilon'' < 1$ in the NIR due to a high density (~ 4×10^{20} cm^{-3}) and mobility (~ 20 cm^2/Vs) of free charge carriers. Thus, NIR plasmonics (propagating and localized surface plasmon modes) may be studied

with M:ZnO layers, nanoparticles, and other nanostructures. Novel metamaterials and applications, such as superresolution systems and other transformation-optics and molecular fingerprint photonic sensors may be developed employing these metal doped oxide materials.

Acknowledgements

We acknowledge the support of the Sectoral Operational Programme Human Resources Development 2007-2013 of the Romanian Ministry of Labor, Family and Social Protection through the Financial Agreement POSDRU/88/1.5/S/60203. Financial support by the European Research Council (Starting Grant “ActiveNP”, 257158) is acknowledged. Purdue co-authors acknowledge support from ONR MURI grant N00014-10-1-0942.

Table captions

Table 1:
Sintering parameters and some physical properties of ZnO ceramics containing Al_2O_3 (0 - 5 wt%) or Ga_2O_3 additions (0 - 7 wt%). Metal oxide powders of Alfa Aesar (AA) and Acros Organics (AO) are used in ceramics fabrication.

Figure captions

Figure 1:
Optical transmission of Al:ZnO (a) and Ga:ZnO (b) thin films on glass substrates measured under perpendicular incidence. Calculated transmission of metal doped ZnO films (solid lines “sim1”) and of undoped pure ZnO films (dashed lines “sim2”).

Figure 2:
Spectroscopic ellipsometric parameters Δ (a) and Ψ (b) of Al:ZnO thin film (2 wt%) on glass substrate. Angle of incidence AOI is 60° and 70°. Measured parameters (solid lines), fitted parameters (dashed lines).

Figure 3:
Dielectric permittivity of Al:ZnO (2 wt%), Ga:ZnO (2 wt%), and pure ZnO (0 wt%) thin films obtained from fits to SE data. Real part ε' (solid symbols) and imaginary part ε'' (open symbols) of films.

Figure 4:
Crossover wavelengths λ_c (a) and imaginary permittivity at this wavelength $\varepsilon''(\lambda_c)$ (b) for Al:ZnO and Ga:ZnO thin films on glass depending on M_2O_3 concentration in ceramic targets.

REFERENCES

[1] D. P. Norton, Y. W. Heo, M. P. Ivill, K. Ip, S. J. Pearton, M. F. Chisholm, T. Steiner, Materials Today (June 2004) 34.

[2] Ü. Özgür, Ya. I. Alivov, C. Liu, A. Teke, M. A. Reshchikov, S. Doğan, V. Avrutin, S.-J. Cho, H. Morkoç, Journal of Applied Physics **98**, 041301 (2005)

[3] S.F. Yu, C. Yuen, S.P. Lau, Y.G. Wang, H.W. Lee, B.K. Tay, Applied Physics Letters **83**, 4288-4290 (2003)

[4] T. Minami, Semicond. Sci. Technol. **20** (2005) S35.

[5] S.-M. Park, T. Ikegami, K. Ebihara, Japanese Journal of Applied Physics **44**, 8027-8031 (2005)

[6] M. Hiramatsu, K. Imaeda, N. Horio, M. Nawata, J. Vac. Sci. Technol. A **16**, 669-673 (1998)

[7] H. Agura, A. Suzuki, T. Matsushita, T. Aoki, M. Okuda, Thin Solid Films **445**, 263-267 (2003)

[8] H. Kim, A. Piqué, J.S. Horwitz, H. Murata, Z.H. Kafafi, C.M. Gilmore, D.B. Chrisey, Thin Solid Films **377-378**, 798-802 (2000)

[9] P. Kuppusami, G. Vollweiler, D. Rafaja, K. Ellmer, Applied Physics A **80**, 183-186 (2005)

[10] K.-K. Kim, S. Niki, J.-Y. Oh, J.-O. Song, T.-Y. Seong, S.-J. Park, S. Fujita, S.-W. Kim, Journal of Applied Physics **97**, 066103 (2005)

[11] R.J. Mendelsberg, S.H.N. Lim, Y.K. Zhu, J. Wallig, D.J. Milliron, A. Anders, Journal of Physics D: Applied Physics **44**, 232003 (2011)

[12] J. Clatot, G. Campet, A. Zeinert, C. Labrugère, A. Rougier, Applied Surface Science **257**, 5181-5184 (2011)

[13] A. Ohtomo, A. Tsukazaki, Semicond. Sci. Technol. **20**, S1-S12 (2005)

[14] S.-M. Park, T. Ikegami, K. Ebihara, Thin Solid Films **513**, 90-94 (2006)

[15] M.-S. Oh, D.-K. Hwang, D.-J. Seong, H.-S. Hwang, S.-J. Park, E.D. Kim, Journal of The Electrochemical Society **155**, D599-D603 (2008)

[16] A. Boltasseva, H.A. Atwater, Science **331**, 290-291 (2011)

[17] P.R. West, S. Ishii, G.V. Naik, N.K. Emani, V.M. Shalaev, A. Boltasseva, Laser Photonics Review **4**, 795–808 (2010)

[18] G.V. Naik, J. Kim, A. Boltasseva, Optical Materials Express **1**, 1090–1099 (2011)

[19] D. Bäuerle, Laser Processing and Chemistry, 4th edition, Springer (2011)

[20] A. Vlad, S. Yakunin, E. Kolmhofer, V. Kolotovska, L. Muresan, A. Sonnleitner,

D. Bäuerle, J.D. Pedarnig, Thin Solid Films **518**, 1350-1354 (2009)

[21] E. Dumont, B. Dugnoille, S. Bienfait, Thin Solid Films **353**, 93-99 (1999)

[22] www.newport.com

[23] R.L. Weiher, Physical Review 152, 736-739 (1966)

[24] Z. Qiao, C. Agashe, D. Mergel, Thin Solid Films **496**, 520-525 (2006)

[25] H. Fujiwara, Spectroscopic Ellipsometry: Principles and Applications, John Wiley & Sons Inc, ISBN 0-470-01608-6 (2007)

[26] A. Ganjoo, R. Golovchak, Journal of Optoelectronics and Advanced Materials **10**, 1328-1332 (2008)

[27] G.V. Naik, A. Boltasseva, Metamaterials **5**, 1–7 (2011)

[28] A.C. Gâlcă, M. Secu, A. Vlad, J.D. Pedarnig, Thin Solid Films **518**, 4603-4606 (2010)

[29] Z.L. Wang, Journal of Physics: Condensed Matter **16**, R829–R858 (2004)

[30] C. Klingshirn, ChemPhysChem **8**, 782-803 (2007)

[31] B.Q. Cao, J. Zúniga-Pérez, N. Boukos, C. Czekalla, H. Hilmer, J. Lenzner, A. Travlos, M. Lorenz, M. Grundmann, Nanotechnology **20**, 305701 (2009)

Table 1:

M:ZnO ceramics	Al_2O_3			Ga_2O_3		
M_2O_3 supplier	AA	AA	AO	AA	AA	AA
temperature [° C]	1000	1000	1000	1000	900	600
time [h]	5	16	5	5	2	5
density [g/cm^3]	5.3	4.9	4.55	4.7	4.05	3.2
color	green	grey	yellow	yellow	yellow	white

Table 1,
M.A. Bodea et al, Applied Physics A (published 2013, published online 2012)

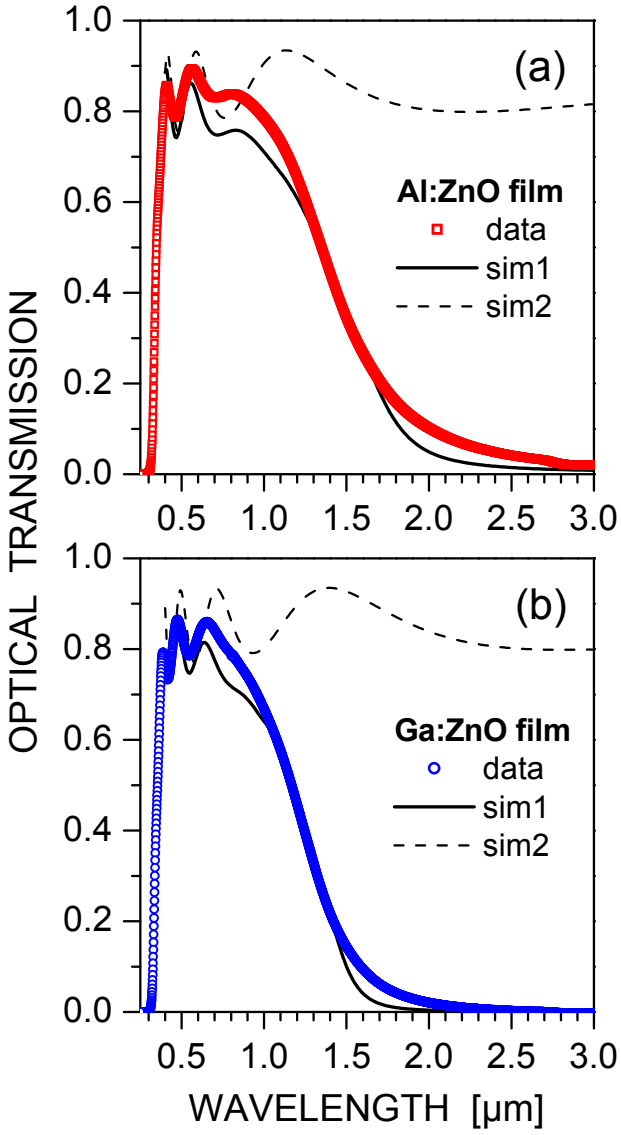

Figure 1,
M.A. Bodea et al, Applied Physics A (published 2013, published online 2012)

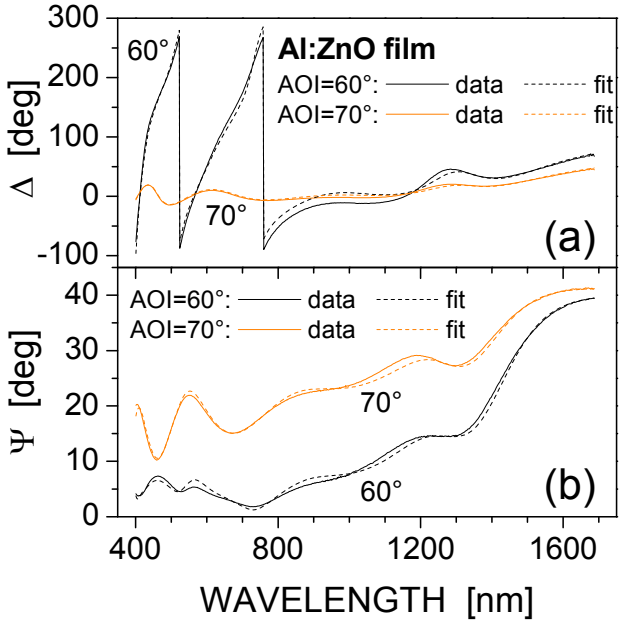

Figure 2,
M.A. Bodea et al, Applied Physics A (published 2013, published online 2012)

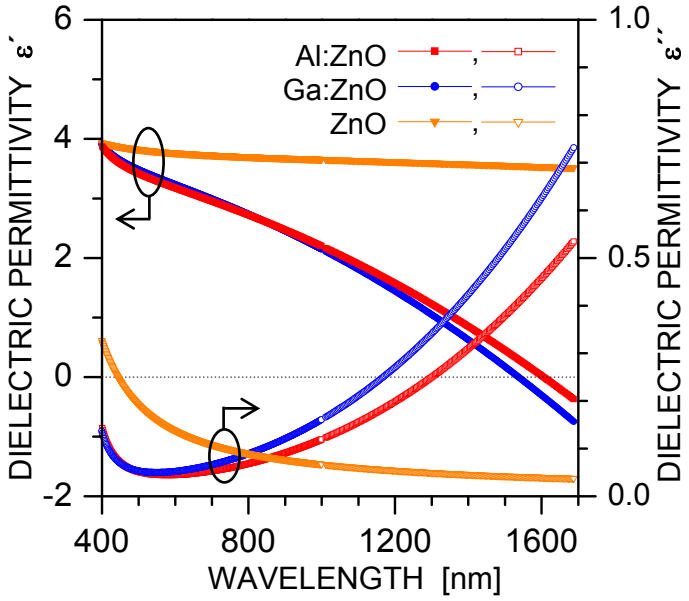

Figure 3,
M.A. Bodea et al, Applied Physics A (published 2013, published online 2012)

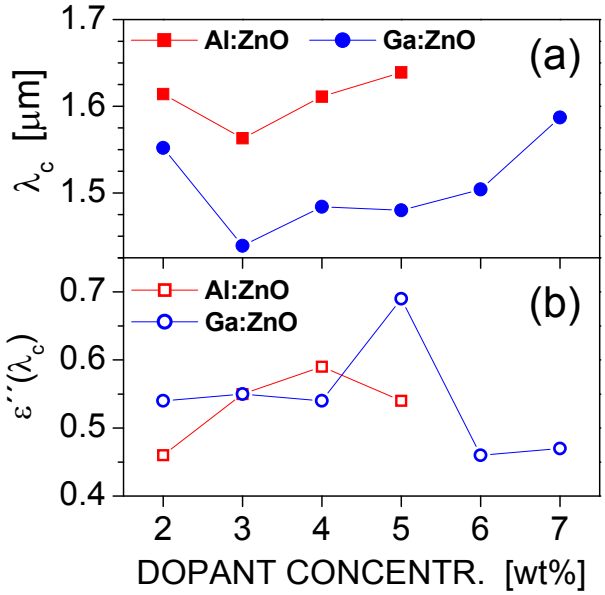

Figure 4,
M.A. Bodea et al, Applied Physics A (published 2013, published online 2012)